

Lamellar Structures of MUC2-Rich Mucin: A Potential Role in Governing the Barrier and Lubricating Functions of Intestinal Mucus

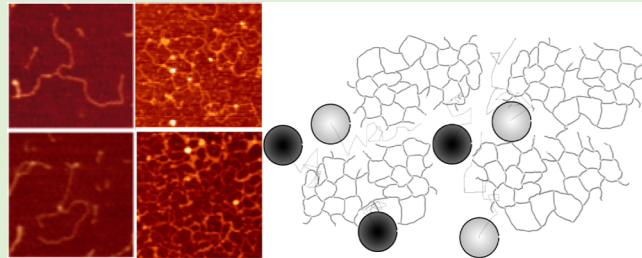
Andrew N. Round,^{*,†} Neil M. Rigby,[‡] Angela Garcia de la Torre,[§] Adam Macierzanka,[‡] E. N. Clare Mills,^{‡,||} and Alan R. Mackie[‡]

[†]School of Pharmacy, University of East Anglia, Norwich Research Park, Norwich NR4 7TJ, U.K.

[‡]Institute of Food Research, Norwich Research Park, Colney Lane, Norwich Research Park, Norwich NR4 7UA, U.K.

[§]Clinical Chemistry Service, University Hospital Virgen de la Victoria, 29010 Malaga, Spain

ABSTRACT: Mucus is a ubiquitous feature of mammalian wet epithelial surfaces, where it lubricates and forms a selective barrier that excludes a range of particulates, including pathogens, while hosting a diverse commensal microflora. The major polymeric component of mucus is mucin, a large glycoprotein formed by several MUC gene products, with MUC2 expression dominating intestinal mucus. A satisfactory answer to the question of how these molecules build a dynamic structure capable of playing such a complex role has yet to be found, as recent reports of distinct layers of chemically identical mucin in the colon and anomalously rapid transport of nanoparticles through mucus have emphasized. Here we use atomic force microscopy (AFM) to image a MUC2-rich mucus fraction isolated from pig jejunum. In the freshly isolated mucin fraction, we find direct evidence for trigonally linked structures, and their assembly into lamellar networks with a distribution of pore sizes from 20 to 200 nm. The networks are two-dimensional, with little interaction between lamellae. The existence of persistent cross-links between individual mucin polypeptides is consistent with a non-self-interacting lamellar model for intestinal mucus structure, rather than a physically entangled polymer network. We only observe collapsed entangled structures in purified mucin that has been stored in nonphysiological conditions.



INTRODUCTION

Mucus forms a protective and selective barrier as well as a lubricating film over wet epithelial surfaces in the mammalian body, including those of the respiratory, ocular, reproductive, and gastrointestinal (GI) systems.^{1,2} It consists of large glycoproteins (mucins) forming a viscoelastic gel. While many details of the structure of individual mucin polymers are well understood,³ and many observations of the micro and macroscale rheology of mucus have been made,^{4–10} it is apparent that there currently remain significant gaps in our understanding of the way in which the secreted mucin polymers are arranged so as to give rise to their observed behavior.¹¹ A clearer understanding of this link will critically inform our understanding of how the mucus barrier works: how commensal and pathogenic bacteria interact with the mucosal environment, how drug delivery across the mucus barrier may be affected, and how physiological processes such as nutrient absorption after digestion take place. In particular, the prevailing view of GI mucins forming a shear-thinning, physically entangled gel is not a convincing model that allows mucus in the GI tract to act both as a barrier and as a lubricating layer if there are extensive cross-links between the mucins. Recent evidence suggests that protease-resistant trimeric cross-links are formed at the N-termini of MUC2 mucins,¹² the dominant mucin gene product in the small and large intestine, and so the model of GI mucin needs to be

revisited if we are to form a clear picture of its function as a barrier and lubricant.

Recently, several new findings have highlighted this gap in our understanding and emphasized the benefits of gaining a detailed insight into the molecular and supramolecular mechanisms underpinning mucus behavior. Following the observations^{7–10} that nonmucoadhesive nanoparticles as large as 500 nm were able to diffuse through cervicovaginal mucus at rates only 4–6 times slower than through water, and that the simultaneous presence of small mucoadhesive particles increased the diffusion of the nonmucoadhesive particles through the mucus, Macierzanka et al. recently observed that similarly sized particles diffuse relatively freely in intestinal mucus when bile salts are absorbed to the particles.⁶ To account for their observations in cervicovaginal mucus, Lai et al.^{7–10} fitted their particle trajectories to a model based upon diffusion in an isotropic gel system with a single characteristic mesh size¹³ and proposed that the mucin network must therefore consist of much larger pores (>400 nm) than had previously been shown. A key difference between the mucus of the small and large intestine on the one hand, and that of the gastric, salivary, ocular, respiratory and cervicovaginal epithelia

Received: July 4, 2012

Revised: August 22, 2012

Published: September 16, 2012

on the other, is the identity of the genes coding for the peptide cores of the secreted, gel-forming mucins. Intestinal secreted mucins are predominantly MUC2, whereas the secreted mucins in the other systems are largely MUCSAC, MUC5B, and MUC6.^{14–20} That this difference has consequences for the microstructures of the mucus gels they form is suggested by evidence that the N-termini of MUC2 form protease-resistant trimers,¹² although no direct evidence for the existence of these trimers in native mucins isolated from intestinal mucus has been found.²¹ Recently, it has been shown that N-terminal fragments of MUC2 transfected into a human colon carcinoma cell line (LS174T) are involved in the pH- and Ca²⁺-mediated unpacking of mucin upon secretion from goblet cells.²² It is difficult to envisage a lubricating role for a heavily cross-linked gel system, such as that which will arise in a covalently linked trimeric structure, unless the extent of cross-linking is in some way modulated. Johansson et al.^{23–25} have shown that in the mammalian colon, MUC2 mucin is present in two different layers: a dense, stratified layer at the epithelium in which no bacteria are found, and a looser, mixed layer that hosts a diverse mucosal flora. Intriguingly, the mucins present in each layer appear to be identical, suggesting that the very different properties of the two layers are the result of other factors, such as nonmucin components of the mucus. A model that views mucin as an isotropic cross-linked network does not predict these features, and so we set out to examine the conformations of single polymers of the mucins present in mucus from the porcine jejunum and the networked gel structures they form.

In this work, we use atomic force microscopy (AFM) to image mucin isolated from pig jejunum at the nanoscale. AFM has been used successfully to characterize conformational and hydrodynamic properties of individual mucin polymers,^{26–29} to follow pH-induced changes in gel structure in gastric mucins³⁰ and to probe the distribution of different glycoforms of MUCSAC in the human ocular tear film.³¹ Using established preparation techniques^{32,33} we isolate mucin from the jejunal mucus and image it with AFM.

MATERIALS AND METHODS

Collection and Preparation of Porcine Jejunal Mucin. Fresh porcine small intestine, obtained from a local slaughterhouse, was rinsed with 67 mM phosphate buffer (pH 6.7) containing 0.02% w/v sodium azide and a mix of protease inhibitors (Roche Diagnostics GmbH, Mannheim, Germany; 1 tablet per 50 mL buffer) to remove debris. Mucus was removed by scraping the epithelial surface of the jejunum segment of the intestine with a plastic scraper (Corning, NY). Extraneous debris (such as dead epithelial cells) was removed by extracting the ex vivo mucus overnight at 18–22 °C with gentle (30 rpm) stirring in 7 volumes of extraction buffer (10 mM sodium phosphate, pH 6.5, containing 4 M guanidinium hydrochloride, 5 mM EDTA, 5 mM N-ethylmaleimide and 0.02% w/v sodium azide). The mucus solution was adjusted to a density of 1.4 g/mL with CsCl and centrifuged (55K rpm at 10 °C for 62 h). Aliquots of 0.5 mL were sampled, absorption at 280 nm was measured, and 2 μL of each fraction was spotted and stained with Alcian blue. UV and Alcian blue-positive aliquots were pooled and diluted in extraction buffer lacking guanidinium hydrochloride (final guanidinium concentration 0.5 M), adjusted in density to 1.41 g/mL with CsCl, and centrifuged again (50K rpm at 10 °C for 96 h). One milliliter aliquots were sampled, measured at 280 nm, and stained with Alcian blue. The fraction at 1.55–1.6 g/mL was strongly Alcian blue-positive and had very weak absorption at 280 nm, identifying it as the mucin fraction. This fraction was dialyzed against phosphate-buffered saline (PBS; 10 kDa tubing) and stored at 4 °C before use.

Dry Weight Determination of Purified Mucin. Aliquots of the purified mucin (ca. 100 mg) were placed in preweighed, clean, and dry aluminum pans. The weight of the pan with the wet sample was recorded to 1 μg using a Mettler ME30 balance. Mucin samples were dried in an oven heated to 65 °C for at least 24 h followed by cooling in a desiccator for at least 30 min prior to weighing. Samples were placed back into the oven, and the cycle was repeated until successive weight differences were less than 3%. The weight of the mucin was determined after assaying the dry weight of salts in the pure buffer used in the mucin preparation. The purified mucin was analyzed in triplicate, and the mean of the results was used for further analysis.

AFM Sample Preparation and Imaging. Mucins were imaged using a JPK Nanowizard II AFM (JPK, Berlin, Germany). Olympus silicon cantilevers (Tokyo, Japan) with a nominal spring constant of 42 N/m were used. Mucins stored in a solution containing 500 mM GuHCl were dialyzed against 10 mM HEPES and 10 mM MgCl₂, deposited onto freshly cleaved mica in a 20 mL droplet, allowed to equilibrate for 5 min, rinsed in deionized water (Fluka Riedel-de-Haen, Seelze, Germany), and blown dry using dried nitrogen (N₂) gas. All images were collected in the repulsive regime of intermittent contact mode in air.³⁴ This procedure and the composition of the buffer have been demonstrated to allow mucins and other polymers to adopt equilibrated conformations at the mica surface.^{27,32,35} Length and width measurements of mucins were carried out using WSxM;³⁶ mucin pore areas and deposited film thicknesses were measured using ImageJ.³⁷

RESULTS

Porcine Jejunal Secreted Mucin Is Rich in MUC2.

Mucus secreted by various different epithelial barriers comprises several different MUC gene products, the most common of which are MUC2, MUC5AC, MUC5B, and MUC6.¹ The latter three gene products are oligomerized C–C and N–N and are generally considered to form large, linear glycoproteins decorated with dense regions of glycosylated side chains. The mechanism by which they perform their function in the mucosae where they are found is predicated on these structural attributes. There is evidence, however, that MUC2 secreted in the large intestine adopts a different trigonally linked oligomeric structure, formed by linkages between the N-termini of the constituent MUC2 polypeptides.^{12,22} Mucin was isolated from porcine jejunum following methods described elsewhere⁶ and further fractionated in a gentle manner aimed at retaining as much of the polymeric structure as possible. Immunostaining (Figure 1) using MUC-specific antibody preparations shows that the fraction was dominated by MUC2 with only small amounts of the secreted gel-forming mucins MUC5AC and no detectable amount of MUC6. When considered in the context of our use of established methods for the isolation of mucin polymers from mucus (see Materials and

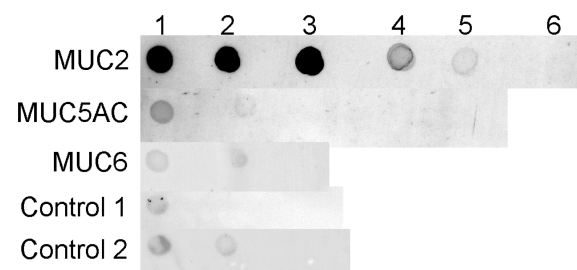


Figure 1. Immunostaining data showing positive for MUC2, minor amounts of MUC5AC and their anti rabbit control 1, and showing negative for MUC6 against its anti goat control 2. The columns represent serial 10-fold dilutions.

Methods and ref 6), the structures we observe in the AFM images will therefore be dominated by MUC2.

Dimensions of Mucin Polymers Measured by AFM.

Individual polymers were identified on the basis of their heights and widths, taking into consideration the well-known distortions induced by the interaction with the AFM probe.^{34,38} Figure 2 shows line traces from AFM images used

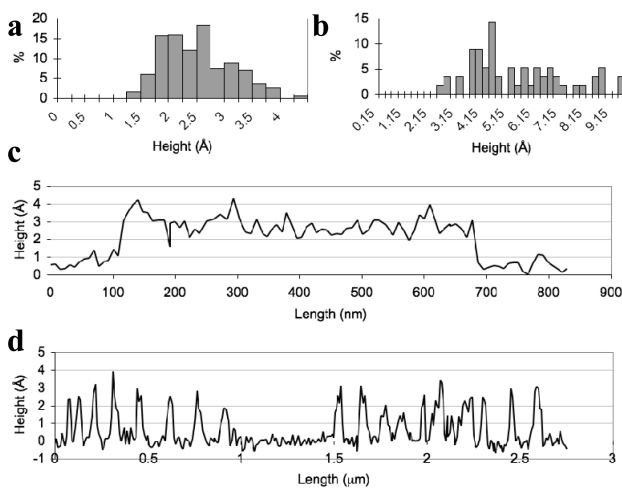


Figure 2. (a) Histogram of heights along individual polymer strands. (b) Histogram of heights along fibrillar bundles of mucin. (c) Line trace along the contour of a single mucin polymer. (d) Line trace across the widths of several single polymers.

to determine the heights and widths of individual mucin polymers and fibril bundles in these samples and conditions, and histograms of the distributions measured. Heights for individual polymers in the images ranged from 0.15 to 0.38 nm, with a mean of 0.23 nm, and the corresponding width range was 23.6 to 44.2 nm, with a mean of 31.4 nm. Heights and widths of fibril bundles are larger and much more broadly distributed.

These values do not directly reflect the hydrated cross-sectional area of a mucin polymer in physiological conditions, but instead are distorted, in accordance with the expected interaction between an AFM probe operating in intermittent contact and a single polymer on a mica substrate. The apparent widths measured here arise from the convolution of the radius of curvature of the end of the probe with the true width of the feature being imaged, and are approximately related to the true width of the feature by $W = (8wR)^{1/2}$ (where W = apparent width measured from the image, w = true width of feature, and R = AFM probe tip radius). The apparent heights are influenced by the imaging force used (strongly dependent on whether the AFM is operating in the attractive or repulsive regimes, which itself is determined by the drive frequency, amplitude, and set point used) and also by the size and shape of the imaging probe. Compression of single polymers to 10% or less of their true height is common. Taking the mean measured height to be 10% of the true value, and assuming a tip radius of 30 nm, we estimate a diameter of approximately 2–3 nm for individual mucin polymers in these samples. This value is in reasonable agreement with a recent estimate of the diameter of MUC2 mucin at 4 nm.²²

MUC2-Rich Mucin Isolated from Porcine Jejunum Forms Linear and Trigonally Linked Polymers and Networks. Our initial goal was to use AFM to determine

whether the trimeric structures observed by Godl et al.¹² when MUC2 N-termini were expressed in CHO cells were present in native MUC2-rich mucin. AFM images of dilute solutions (0.002–0.08 mg/mL dry weight) of the mucins freshly isolated from porcine jejunum show the existence of several levels of organization of mucin oligomers (Figure 3a). These range from individual branched (Figure 3b–e) and linear (Figure 3a,f) oligomers to fragments of a porous network (Figure 3g,h) and features interpreted as partially expanded secreted mucin granules (Figure 3i).

Individual mucin oligomers had lengths ranging from 50 nm to more than 1500 nm, which are comparable with previous

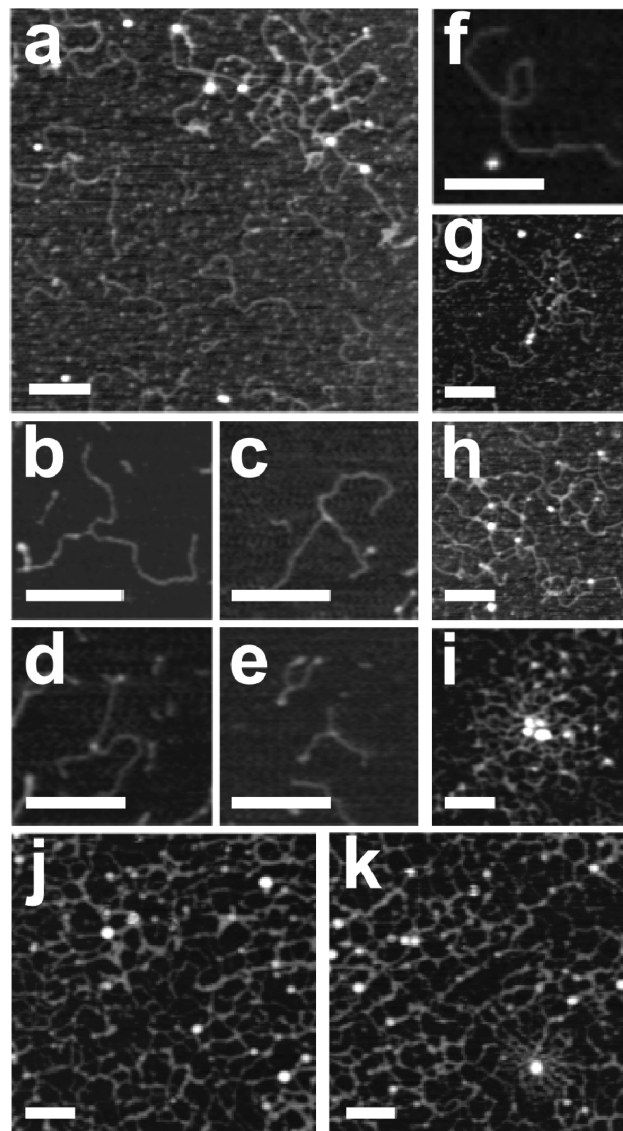


Figure 3. AFM images of porcine jejunal mucin: (a) image of field of mucin polymers, showing the coexistence of individual linear and trimerized MUC-2 oligomers with network fragments (1500 nm^2); (b–e) examples of trimerized MUC-2 oligomers (500 nm^2); (f) an example of a linear polymer, here crossing over itself (500 nm^2); (g,h) examples of network fragments (1000 nm^2); (i) example of a partially expanded granule (1000 nm^2); (j) image of a field of an extensive lamellar network at higher concentration (0.05–0.08 mg dry matter/mL) (1500 nm^2); and (k) a partially expanded mucin granule embedded in the lamellar network (1500 nm^2). Scale bar = 250 nm in all cases.

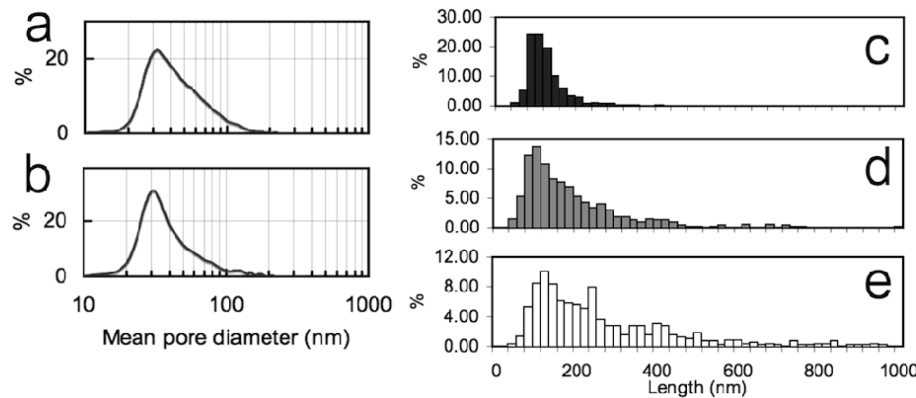


Figure 4. Distributions of pore diameters and mucin strand lengths for freshly isolated purified mucin. Pore diameter distributions for (a) network fragments and (b) dense mucin networks; distributions of interlinkage and individual molecular strand lengths in (c) dense mucin networks, (d) network fragments, and (e) individual mucin oligomers.

direct measurements of the distribution of lengths of individual purified mucin oligomers.^{26–28,39} We observed several cases of apparently branching polymers, in which all three strands entering the junction have dimensions commensurate with single oligomers (Figure 3b,c,d) suggestive of MUC2 mucin trimer formation. Isolated, branched polymers identified in this way were always trimers, and no tetramers or higher order branches, where all the strands emerging from the junction were single mucin oligomers, were observed.

In addition to these discrete linear and trigonally linked structures, assemblages of several polymer strands into networks were commonly observed. These networks were formed predominantly from strands with dimensions commensurate with single MUC-2 oligomers, linked together through cross-links between three, four, or five strands (Figure 3g,h). Again, this observation stands in contrast to previous single molecule microscopic observation of other mucins,^{21,26–28,31,40} in which such networks have not been observed. The mucin samples imaged here also contain examples of features consisting of dense networks of oligomers surrounding a central core and with radii of approximately 1 μm (Figure 3i). They resemble features previously observed for MUC5B⁴⁰ and MUC5AC^{26–28,31} mucins and interpreted as mucin granules caught in the process of expanding and unfolding, in that they form radiating networks around a central core, but differ in that the features observed here show branching between the strands rather than the extended loops characteristic of expanded granules in lung and tear film mucins. Accordingly, we interpret the features observed here as secreted granules of MUC2 mucin undergoing expansion. It is possible that removal of the mucus from the jejunum liberates some intracellular mucin granules that had not yet been secreted.

The observation of isolated trimers of MUC2 coexisting with fragments of a porous network linked by similar trigonal junctions allows us to propose that both structures are remnants of a trigonally linked MUC2 mucin structure from the secreted granules. We tested this by imaging higher concentrations (0.05–0.08 mg/mL) of MUC2-rich mucin, which revealed (Figure 3j,k) extensive regions of mucin networks with strand dimensions commensurate with individual MUC2 oligomers, interspersed with regions where the mucin strands are thicker, suggesting the association of two or more MUC2 oligomers into fibrils. It is striking to note that, even at concentrations giving rise to extensive, apparently contiguous networks over several micrometres, freshly isolated

mucin only forms a thin layer network on the flat mica substrate, and little three-dimensional structure is observed. If this represents the native mucin network structure, then it strongly suggests that trimerization and subsequent trimer association to form a network occur predominantly or exclusively in one plane, to allow the formation of lamellar sheets. Evidence that these are indeed intrinsic to polymeric mucin comes from the observation in Figure 3k that partially expanded granules are sometimes found embedded in the network, shedding some light on the process by which the networks are formed from the unpackaged granules after secretion onto the epithelial surface.

Mesh Sizes in the Mucin Networks at High and Low Concentrations Show Similar Distributions. To further characterize the mucin network, we measured the areas of the pores in the network, and expressed their distribution in terms of the diameters of circular pores with equivalent areas. Figure 4a,b shows pore diameter distributions for the mucin dilutions depicted in Figure 3, encompassing network fragments coexisting with single polymers (such as those depicted in Figure 3a,g,h) as well as the extensive lamellar network shown in Figure 3j-k. Both show similar distributions, ranging from 20 to 200 nm with a pronounced peak at 30 nm. Figure 4c,d,e show length distributions for uninterrupted single chains in three cases: isolated single oligomers (linear or branched, as shown in Figure 3b–f), network fragments (Figure 3a,g,h), and extended lamellar networks (Figure 3j,k). Gaussian peak fitting to these three distributions reveals that all three populations share a common peak at approximately 100 nm. The distribution of lengths found in the extensive network has an upper bound at approximately 250 nm, whereas the network fragments and isolated oligomer length distributions have tails that extend further with decreasing mucin concentration, up to 500 nm in the case of the network fragments and to more than 1 μm for individual oligomers. The distribution of lengths reported here is in line with previous single molecule measurements of mucin oligomer length distributions.^{26–28,39} A network constructed from trimers with unit side lengths of 100 nm would be expected to possess pore diameters of approximately 150 nm; instead we observe a distribution of pore diameters that peaks around 30 nm. This discrepancy arises because our measurement of pore size encompasses the smaller pores of the partially unpacked granules and the pores formed by the bundled fibrils described earlier, whose lengths are excluded from the polymer length analysis where they are

clearly not single chains. This observation suggests that there may exist regions of dense fibrillar assemblies of mucin polypeptides, perhaps reflecting noncovalent interactions between the CysD domains^{41,42} or locally varying counterion concentration caused by the persistent presence of Ca^{2+} ions that condensed the mucin in the granule before secretion, which may be associated with smaller pores.

Polymer Entanglement Only Occurs in Purified Stored Mucin Samples. We observed that, upon storage of the purified mucin (500 mM GuHCl, 10 mM HEPES, pH 7.4, 4 °C for more than four weeks), the nature of the networks formed by the mucins changed, and the lamellar character of their appearance when imaged on mica decreased. Figure 5

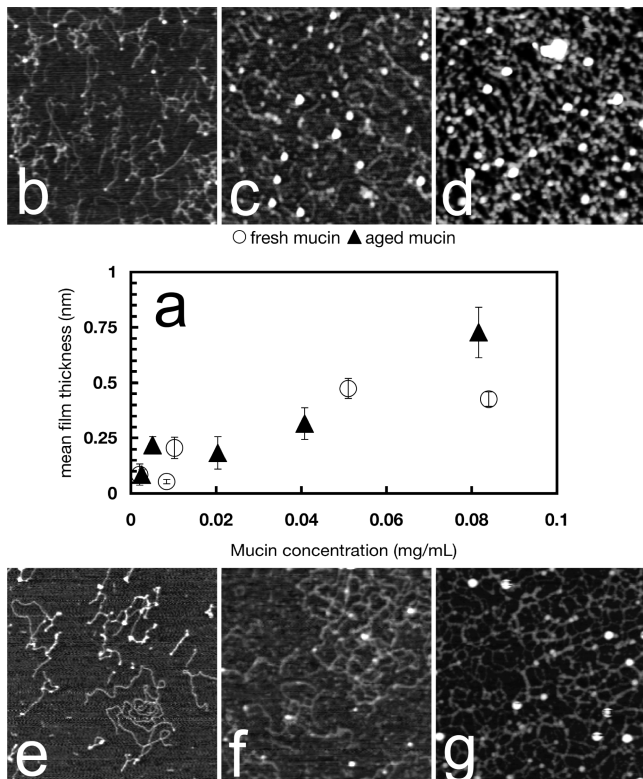


Figure 5. Observing the lack of self-interactions of lamellae in freshly isolated mucin and the onset of polymer entanglement in stored mucin. (a) Thickness of adsorbed mucin film vs mucin concentration deposited for fresh and stored mucin. AFM images of stored mucin at (b) 0.002 mg/mL, (c) 0.04 mg/mL, and (d) 0.08 mg/mL, and fresh mucin deposited at (e) 0.002 mg/mL, (f) 0.05 mg/mL, and (g) 0.08 mg/mL. Images all 1000 nm².

shows how the amount of mucin deposited, and the structures it forms, change when the mucin is stored. At the highest concentrations examined (0.08 mg/mL), mucin that revealed extensive lamellar networks when fresh (Figures 3j,k, and 5g), forms a dense, collapsed, multilayered network with no evidence of porous networks when stored (Figure 5d). Figure 5a shows clearly that at these high concentrations the amount of mucin deposited on the surface when stored is approximately twice as much (0.08 vs 0.04 nm film) as when fresh. Upon dilution to concentrations equivalent to those showing the coexistence of individual MUC2 oligomers and porous network fragments (Figures 3g,h and 5e), images of the stored mucin show a comparatively more heterogeneous surface coverage, with loosely entangled polymers coexisting with denser patches

(Figure 5b). Again, a porous network is less evident than in freshly isolated mucins. Overall we find that when fresh mucin is deposited, once a lamellar network is formed, this inhibits further mucin deposition, whereas when stored mucin is deposited, the amount of material adsorbed depends linearly on the concentration (Figure 5a). Further evidence supporting this conclusion comes from consideration of the pore size distributions for stored mucin samples (Figure 6). At similar

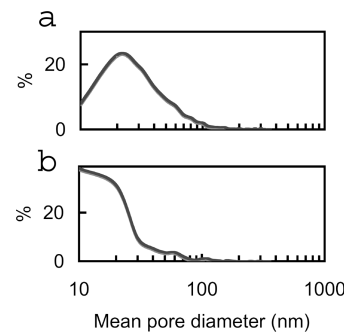


Figure 6. Distributions of pore diameters for stored, purified mucin samples. Pore diameter distributions for concentrations of (a) 0.04 mg/mL and (b) 0.08 mg/mL.

concentrations to those used for the fresh mucin, the distributions of pore sizes in the stored mucin show a pronounced shift to smaller values: at a concentration of 0.04 mg/mL, the peak in the distribution shifted to 20 nm, with a marked increase in pores at 10 nm diameter (Figure 6a), while at a concentration of 0.08 mg/mL, where the trapping of entangled polymers has significantly increased the thickness of the deposited layer, the peak pore size shifted further to 10 nm or below (Figure 6b).

To quantify this change in character of the mucin network, we classified each network junction according to how many strands entered it. Table 1 shows how many strands take part in

Table 1. Number of Strands in Each Junction for Individual Polymers, Network Fragments, Lamellar Networks, and Entangled Polymers from Stored Mucin

	strands per junction (%)		
	3	4	5
individual polymers	100	0	0
network fragments	79	18	3
lamellar networks	75	24	1
entangled polymers	51	37	12

each junction identified for individual polymers, network fragments, lamellar networks, and entangled, stored mucin. We observe that individual polymers do not contain junctions of more than three strands, the network fragments and lamellae overwhelmingly consist of trigonal junctions, and that the amounts of higher order junctions increase on storage, with four or five strands entering a junction frequently. The most likely explanation for four-membered junctions is the superposition of two strands, one across the other, while the five-membered strands observed are always accompanied by dense knots of material at the junction. In the case of the stored mucins, these junctions may reflect entanglement and knotting of the mucin polymers occurring upon deposition and drying. The change in network character on storage suggests that over

time it disassembles as the interactions that hold it together become disrupted.

■ DISCUSSION

Purified Porcine Jejunal MUC2-Rich Mucin Forms Trimers That Are Assembled into Extensive Lamellar Porous Networks. We have shown, for the first time, trimerization of MUC2 oligomers in a MUC2-rich polymeric mucin. This observation is consistent with the fact that both porcine submaxillary mucin (the N-terminus of which shares some homology with MUC2)^{43,44} and the N-terminal portion of human MUC2 expressed in CHO cell lines can form trimers.¹² It was recently shown²² that trimers formed from the N-termini of MUC2 expressed in colonic goblet cell lines are involved in the pH- and Ca²⁺-mediated unpacking and expansion of mucins upon secretion. Our data support the premise that these trimers represent structures found in polymeric mucin and are not artifactually generated as a result of different processing of the mucin oligomers after synthesis in normally nonmucin-producing cell lines.²¹ The other common secreted mucins, MUC5AC, MUC5B, and MUC6, are considered to retain a linear morphology, and no evidence for trigonal formation has been reported for these mucins.^{26–28,31,39} We show that MUC2 trimers are responsible for the formation of a porous, lamellar network of mucin. Figures 3–6 and Table 1 provide evidence that the networks formed by MUC2 mucin are two-dimensional lamellae. The similarity of the distributions of lengths for individual oligomers and pore walls, together with the predominance of trigonal linkages in both single molecules and networks, may be considered in the context of the expected behavior of a three-dimensional network collapsed into two dimensions: here, collapse of one layer onto another below it would increase the number of apparent strands in a junction and simultaneously decrease the apparent sizes of the pores, due to superposition and entanglement of the polymers in the two layers. Indeed, in the purified mucin stored for 4 weeks or more, we see structures consistent with the collapse of an entangled, 3d structure: A linear increase in deposited film thickness with increase in concentration (Figure 5a–d), and a concomitant decrease in the size of the pores (Figure 6) as the deposition of the first polymers traps those with which they are entangled. Instead, in fresh mucin we consistently observe similar distributions of polymer strand length, junction number, and pore size for samples of individual oligomers through to extensive networks. Deposited film thickness reaches a plateau, beyond which no new mucin is deposited, showing that the mucin polymers are not entangled with one another and trapped at the surface. This observation is expected for a lamellar network depositing on a flat surface, and shows that essentially there is no entanglement of mucin oligomers in the freshly isolated state. Deposition of the first lamella inhibits adsorption by more mucin, possibly by screening the charge of the divalent magnesium ions complexed with the mica that provide the adhesive interaction for deposition of the primary layer.

In this study we find that features likely to represent individual MUC2 oligomers have diameters of approximately 2–3 nm and lengths ranging from 50 to more than 1000 nm, with a pronounced peak at 100–120 nm (Figure 4e). The polymer chain distances between trigonal nodes also show a similar peak in their distribution at 100 nm, but with a truncated upper bound at about 500 nm (Figure 4c,d). Similar

distributions of polymer lengths have been observed for human ocular MUC5AC mucin^{26–28} and respiratory mucin.³⁹ This distribution of lengths is significantly shorter than that generally predicted for mucin dimers (²² and elsewhere), but is consistent with distributions obtained for other mucins by similar single molecule measurement techniques.³⁹

There is good evidence that MUC2 forms disulfide-linked trimers during transit through the trans-Golgi network of Goblet cells¹² forming net-like structures that are packaged into the secretory granule. We have shown that extended networks with a similar morphology to these secreted nets can be isolated from polymeric intestinal mucin. Ambort et al.²² and Johansson et al.⁴² recently proposed such a model for MUC2 mucin in the colon using an entirely different approach, predicting and finding functional similarities between the structure of MUC2 N-termini and those of Von Willebrand factor, which possesses analogous N-termini. Our finding in this work of porous, netlike structures strongly resembling this model constitutes further evidence that MUC2 mucin is assembled into lamellar sheets in the intestine.

MUC2 Mucin Networks Contain Channels between Lamellae. The range of pore diameters we report (Figure 4a,b) is consistent with previous reports of mucus mesh size,^{4,5,10} but differs from recent estimates based upon nanoparticle tracking experiments.^{6–9} Nanoparticle tracking experiments monitor the diffusion of particles through the mucus network and require reconstruction from that data of the physical dimensions of the mucus network through which the particles have passed. A model is required to fit the diffusion rates and determine a mesh size for the network that will allow passage of the particles. Olmsted et al.⁴ and Lai et al.⁸ used a model describing homogeneous hydrogels,^{45,46} a model appropriate for a physically entangled linear polymer system. Olmsted found, using macromolecules, viruses, and polystyrene nanoparticles, an apparent pore size of 100–110 nm (agreeing with electron micrographs showing pore sizes of 20–200 nm reported in the same work), while Lai found that the diffusion rates they had recorded for poly(ethylene glycol) (PEG)-coated nanoparticles of sizes up to 500 nm required a pore size of at least 340 ± 70 nm.⁸ Although the mucus used in both these works was cervicovaginal and did not contain MUC2, Macierzanka et al.⁶ observed that nonmucoadhesive nanoparticles as large as 2 μ m were able to diffuse through porcine jejunal mucus containing MUC2 mucin at different rates depending on the local microviscosity of the mucus, including some at similar rates to water, implying an open-structured gel mesh similar to that calculated by Lai et al. It is important to note that Macierzanka et al. reported similar distributions of Stokes viscosities for the 500 nm nonmucoadhesive nanoparticles in both a mucin preparation similar to the one studied in this work and in an ex-vivo mucus sample that had not been purified (and thus reflects the behavior of the mucin in its native mucosal environment). The authors concluded from this that the obstruction to particle diffusivity they observed was due to the mucin and not, to a significant degree, to the presence of other mucus components. Since the mucins used in the present work come from the same source as those used in the work of Macierzanka et al., the structures we observe by AFM reflect those responsible for the behavior reported there. Our observations confirm that the structures formed by mucins that constitute porcine jejunal mucus possess smaller pores in the range 20–200 nm. Thus it is necessary to explain how the nanoparticle transport observed by Macierzanka et al. can occur

when the particles are much larger than the apparent mesh size, particularly since the existence of the covalent trigonal linkages greatly diminishes the system's capacity for shear-thinning. We propose that the key to understanding nanoparticle transport through MUC2 mucin lies in the lamellar structure we identify here, and in particular the nature of the interactions between lamellae. Rather than requiring the mucin gel to possess much larger pores than had previously been observed, our model instead requires that there be only weak interactions between the mucin lamellae. When this condition is met, the mucin will possess transient channels between lamellae, allowing the relatively unhindered passage of large noninteracting particles, not through the pores in the lamellae, but through the channels between the individual lamellae. Figure 7 shows how these lamellae would interact with nanoparticles of varying size and surface chemistry.

Our prediction that nonmucoadhesive particles may bypass the small pores of the network by following interlamellar channels also suggests a mechanism for lubrication similar to

the traditional picture of graphite interlamellar lubrication,⁴⁷ whereby individual lamellae slide past each other. The inhibition of further deposition of mucin after the formation of a 0.5 nm-thick film in freshly isolated mucin samples (Figure S) demonstrates the lack of any significant adhesive interactions between lamellae. The conventional model for mucin lubrication views mucin as an entangled linear polymer solution.^{48,49} Depending on its concentration, such a solution can form a dense gel network or a dilute, shear-thinning solution so long as the linkages between polymers in the network are labile.⁵⁰ However, the key linkages between the MUC2 oligomers involved in trimer formation are covalent disulfide bonds and are known to be protease resistant.¹² Such linkages will limit the ability of MUC2 to act as a lubricant by the same mechanism as other large secreted mucins, such as MUC5AC or MUC5B. Instead, the presence of nonadhesive lamellae implies the model of lamellar lubrication we propose here.

CONCLUSIONS

In summary, we have used a single-molecule technique to image individual molecules of porcine small intestine MUC2 mucins and the networks they form. Direct microscopic visualization of individual molecules reveals that MUC2 mucins form trimers, and that these trimers are the fundamental units of a porous, lamellar network. Characterization of the distributions of pore sizes, lengths of individual oligomers and networked strands, and numbers of strands participating in each network junction all support the hypothesis that the lamellar network is composed of trigonally linked mucins. The extent to which continuous single monolayer networks are observed suggests that the networks are pseudo two-dimensional, with little interaction between lamellae. That very little three-dimensional structure is observed even at high concentrations of mucin suggests that these lamellae interact with each other only weakly, at least in the absence of the physiological mucosal environment and its protein complement. Upon storage, this network breaks down, and a collapsed entangled network is observed.

The presence of protease-resistant trimeric linkages in MUC2-rich mucin challenges the applicability of the shear-thinning, entangled linear polymer model that describes other mucins, such as those in the cervicovaginal tract, to this system: the shear-thinning property depends upon the lability of the cross-links in the polymer solution. A heavily cross-linked polymer gel system would not possess mucus' lubricative properties, so, instead, an alternative mechanism is required. The lack of strong interactions between lamellae of MUC2 mucin implies the existence of channels between lamellae that, if reproduced *in vivo*, would allow the relatively unhindered passage of large nonmucoadhesive particles while maintaining a barrier against bacteria. Evidence that this may indeed be the case arises from the similarity in distributions of Stokes viscosities in ex-vivo mucus and purified mucins from pig jejunal mucus, as observed previously in nanoparticle tracking experiments.⁶ Since the mucin in the colon is also MUC2, and since Ambort et al.²² have proposed a model for colonic mucin structure that shares many features with the one presented here, such a mechanism may also account for the sharp interface between the stratified, tightly adherent, and loose outer MUC2 mucus layers in the colon observed by Johansson et al.^{23–25} Mice lacking MUC2, and thus lacking the tightly adherent layer, display symptoms resembling colitis, suggesting

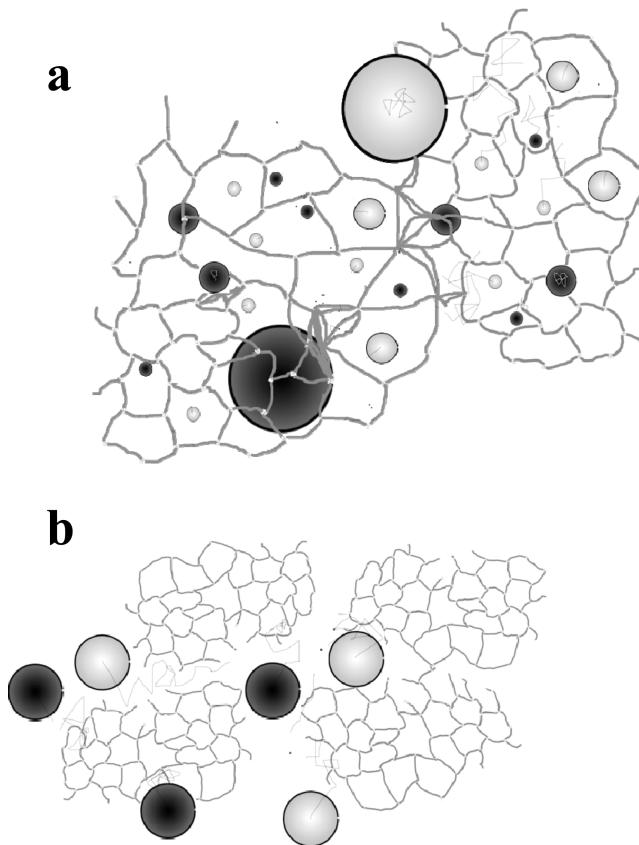


Figure 7. Cartoons graphically depicting the model of individual several-micrometer-sized lamellae in solution, interacting with macromolecules and mucoadhesive particles, while allowing passage of large noninteracting particles between lamellae. Light circles are nonmucoadhesive nanoparticles, and dark circles are mucoadhesive nanoparticles, while thin lines reflect possible paths of the nanoparticles. (a) According to their size, nonmucoadhesive nanoparticles pass freely through the lamellae, not interacting with the mucin until sterically trapped. Mucoadhesive nanoparticles are trapped when they first interact with the mucin network. (b) Nonmucoadhesive nanoparticles of much larger diameters than the mucin pores pass along transient channels between lamellae rather than through the networks. Mucoadhesive nanoparticles follow the same route but are again trapped upon first interaction with mucin.

that this dense mucus barrier plays a crucial role in protecting the colonic epithelium and the lamellar model suggests that interlamellar interactions may govern the transition between layers. Noninteraction between lamellae also suggests an alternative model for the lubricating function of this mucin, allowing the adoption of a graphite-like sliding lamellae mode of lubrication. Elucidating the nature and extent of any annealing of individual mucin granules into extensive lamellae, and of the interactions between lamellae, therefore becomes fundamental to understanding how MUC2 mucin structures are formed, perform their function as a selectively permeable barrier and lubricant, and break down for removal, in the GI tract.

AUTHOR INFORMATION

Corresponding Author

*Telephone: +44 1603 593392; e-mail: a.round@uea.ac.uk

Present Address

[†]School of Translational Medicine, Manchester Academic Health Science Centre, Manchester Institute of Biotechnology, University of Manchester, 131 Princess Street, Manchester M1 7DN, UK.

Author Contributions

The manuscript was written through contributions of all authors. All authors have given approval to the final version of the manuscript.

Notes

The authors declare no competing financial interest.

ACKNOWLEDGMENTS

A.N.R. holds an RCUK Academic Fellowship, and the authors at IFR (N.M.R., A.M., E.N.C.M., and A.R.M.) would like to acknowledge the BBSRC for their support of this work through the Food and Health Strategic Programme Grant to the Institute. A.G.d.I.T. received funding for a research internship in A.N.R.'s lab from the Regional Ministry for Health Andalusia.

REFERENCES

- (1) Linden, S. K.; Sutton, P.; Karlsson, N. G.; Korolik, V.; McGuckin, M. A. *Mucosal Immunol.* **2008**, *1*, 183–197.
- (2) Hansson, G. C. *Curr. Opin. Microbiol.* **2012**, *15*, 57–62.
- (3) Bansil, R.; Turner, B. S. *Curr. Opin. Colloid Interface Sci.* **2006**, *11*, 164–170.
- (4) Olmsted, S. S.; Padgett, J. L.; Yudin, A. I.; Whaley, K. J.; Moench, T. R.; Cone, R. A. *Biophys. J.* **2001**, *81*, 1930–1937.
- (5) Cone, R. A. *Adv. Drug Delivery Rev.* **2009**, *61*, 75–85.
- (6) Macierzanka, A.; Rigby, N.; Corfield, A.; Wellner, N.; Böttger, F.; Mills, E.; Mackie, A. *Soft Matter* **2011**, *7*, 8077.
- (7) Lai, S. K.; O'Hanlon, D. E.; Harrold, S.; Man, S. T.; Wang, Y.-Y.; Cone, R. A.; Hanes, J. *Proc. Natl. Acad. Sci. U.S.A.* **2007**, *104*, 1482–1487.
- (8) Lai, S. K.; Wang, Y.-Y.; Hida, K.; Cone, R. A.; Hanes, J. *Proc. Natl. Acad. Sci. U.S.A.* **2010**, *107*, 598–603.
- (9) Lai, S. K.; Wang, Y.-Y.; Cone, R. A.; Wirtz, D.; Hanes, J. *PLoS ONE* **2009**, *4*, e4294.
- (10) Lai, S. K.; Wang, Y.-Y.; Wirtz, D.; Hanes, J. *Adv. Drug Delivery Rev.* **2009**, *61*, 86–100.
- (11) Thornton, D. J.; Sheehan, J. K. *Proc. Am. Thorac. Soc.* **2004**, *1*, S4–S61.
- (12) Godl, K.; Johansson, M. E. V.; Lidell, M. E.; Mörgelin, M.; Karlsson, H.; Olson, F. J.; Gum, J. R.; Kim, Y. S.; Hansson, G. C. *J. Biol. Chem.* **2002**, *277*, 47248–47256.
- (13) Amsden, B.; Turner, N. *Biotechnol. Bioeng.* **1999**, *65*, 605–610.
- (14) Corfield, A. P.; Carroll, D.; Myerscough, N.; Probert, C. *Front. Biosci.* **2001**, *6*, D1321–D1357.
- (15) McKenzie, R.; Jumblatt, J.; Jumblatt, M. *Invest. Ophthalmol. Vis. Sci.* **2000**, *41*, 703–708.
- (16) Turner, B. S.; Bhaskar, K. R.; Hadzopoulou-Cladaras, M.; Specian, R. D.; LaMont, J. T. *Biochem. J.* **1995**, *308* (Pt 1), 89–96.
- (17) Gipson, I. K.; Ho, S. B.; Spurr-Michaud, S. J.; Tisdale, A. S.; Zhan, Q.; Torlakovic, E.; Pudney, J.; Anderson, D. J.; Toribara, N. W.; Hill, J. A. *Biol. Reprod.* **1997**, *56*, 999–1011.
- (18) Gipson, I. K.; Inatomi, T. *Prog. Retinal Eye Res.* **1997**, *16*, 81–98.
- (19) Thornton, D. J.; Carlstedt, I.; Howard, M.; Devine, P.; Price, M.; Sheehan, J. K. *Biochem. J.* **1996**, *316*, 967–975.
- (20) Dasari, S.; Pereira, L.; Reddy, A. P.; Michaels, J.-E. A.; Lu, X.; Jacob, T.; Thomas, A.; Rodland, M.; Roberts, C. T.; Gravett, M. G.; Nagalla, S. R. *J. Proteome Res.* **2007**, *6*, 1258–1268.
- (21) Thornton, D. J.; Rousseau, K.; McGuckin, M. A. *Annu. Rev. Physiol.* **2008**, *70*, 459–486.
- (22) Ambort, D.; Johansson, M. E. V.; Gustafsson, J. K.; Nilsson, H. E.; Ermund, A.; Johansson, B. R.; Koeck, P. J. B.; Hebert, H.; Hansson, G. C. *Proc. Natl. Acad. Sci. U.S.A.* **2012**, *109*, 5645–5650.
- (23) Johansson, M. E. V.; Phillipson, M.; Petersson, J.; Velcich, A.; Holm, L.; Hansson, G. C. *Proc. Natl. Acad. Sci. U.S.A.* **2008**, *105*, 15064–15069.
- (24) Johansson, M. E. V.; Gustafsson, J. K.; Sjöberg, K. E.; Petersson, J.; Holm, L.; Sjövall, H.; Hansson, G. C. *PLoS ONE* **2010**, *5*, e12238.
- (25) Johansson, M. E. V.; Larsson, J. M. H.; Hansson, G. C. *Proc. Natl. Acad. Sci. U.S.A.* **2011**, *108* (Suppl 1), 4659–4665.
- (26) McMaster, T. J.; Berry, M.; Corfield, A. P.; Miles, M. J. *Biophys. J.* **1999**, *77*, 533–541.
- (27) Round, A.; Berry, M.; McMaster, T. J.; Stoll, S.; Gowers, D.; Corfield, A. P.; Miles, M. J. *Biophys. J.* **2002**, *83*, 1661–1670.
- (28) Round, A.; Berry, M.; McMaster, T. J.; Corfield, A. P.; Miles, M. J. *J. Struct. Biol.* **2004**, *145*, 246–253.
- (29) Brayshaw, D. J.; Berry, M.; McMaster, T. J. *Ultramicroscopy* **2004**, *100*, 145–151.
- (30) Hong, Z.; Chasan, B.; Bansil, R.; Turner, B. S.; Bhaskar, K.; Afshar, N. *Biomacromolecules* **2005**, *6*, 3458–3466.
- (31) Round, A.; McMaster, T. J.; Miles, M. J.; Corfield, A. P.; Berry, M. *Glycobiology* **2007**, *17*, 578–585.
- (32) Hansma, H. G.; Laney, D. E. *Biophys. J.* **1996**, *70*, 1933–1939.
- (33) Brayshaw, D. J.; Berry, M.; McMaster, T. J. *Ultramicroscopy* **2003**, *97*, 289–296.
- (34) Round, A.; Miles, M. J. *Nanotechnology* **2004**, *15*, S176–S183.
- (35) Rivetti, C.; Guthold, M.; Bustamante, C. *J. Mol. Biol.* **1996**, *264*, 919–932.
- (36) Horcas, I.; Fernández, R.; Gómez-Rodríguez, J. M.; Colchero, J.; Gómez-Herrero, J.; Baro, A. M. *Rev. Sci. Instrum.* **2007**, *78*, 013705.
- (37) Schneider, C. A.; Rasband, W. S.; Eliceiri, K. W. *Nat. Methods* **2012**, *9*, 671–675.
- (38) Santos, S.; Barcons, V.; Christenson, H. K.; Font, J.; Thomson, N. H. *PLoS ONE* **2011**, *6*, e23821.
- (39) Sheehan, J. K.; Thornton, D. J.; Howard, M.; Carlstedt, I.; Corfield, A.; Paraskeva, C. *Biochem. J.* **1996**, *315*, 1055–1060.
- (40) Kesimer, M.; Makhov, A. M.; Griffith, J. D.; Verdugo, P.; Sheehan, J. K. *Am. J. Physiol.: Lung Cell. Mol. Physiol.* **2010**, *298*, L15–L22.
- (41) Ambort, D.; van der Post, S.; Johansson, M. E. V.; MacKenzie, J.; Thomsson, E.; Krengel, U.; Hansson, G. C. *Biochem. J.* **2011**, *436*, 61–70.
- (42) Johansson, M. E. V.; Ambort, D.; Pelaseyed, T.; Schütte, A.; Gustafsson, J. K.; Ermund, A.; Subramani, D. B.; Holmén-Larsson, J. M.; Thomsson, K. A.; Bergström, J. H.; van der Post, S.; Rodriguez-Piñeiro, A. M.; Sjövall, H.; Bäckström, M.; Hansson, G. C. *Cell. Mol. Life Sci.* **2011**, *68*, 3635–3641.
- (43) Perez-Vilar, J.; Eckhardt, A. E.; DeLuca, A.; Hill, R. L. *J. Biol. Chem.* **1998**, *273*, 14442–14449.
- (44) Perez-Vilar, J.; Hill, R. L. *J. Biol. Chem.* **1998**, *273*, 34527–34534.
- (45) Amsden, B. *Macromolecules* **1998**, *31*, 8382–8395.

- (46) Amsden, B. *Macromolecules* **1999**, *32*, 874–879.
- (47) Bragg, W. *Bragg (1928) An Introduction to Crystal Analysis*; G. Bell and Sons, Ltd.: London, 1928.
- (48) Dedinaite, A. *Soft Matter* **2011**, *8*, 273.
- (49) Coles, J. M.; Chang, D. P.; Zauscher, S. *Curr. Opin. Colloid Interface Sci.* **2010**, *15*, 406–416.
- (50) Cu, Y.; Saltzman, W. M. *Adv. Drug Delivery Rev.* **2009**, *61*, 101–114.